

1 PREPARED FOR SUBMISSION TO JINST
2 22ND INTERNATIONAL WORKSHOP ON RADIATION IMAGING DETECTORS
3 27TH JUNE 2021 TO 1ST JULY 2021
4 GHENT, BELGIUM (ONLINE)

5 **Development, construction and tests of the Mu2e** 6 **electromagnetic calorimeter mechanical structures**

7 **N. Atanov¹, V. Baranov¹, L. Borrel², C. Bloise³, J. Budagov¹, S. Ceravolo³, F. Cervelli⁴, F.**
8 **Colao⁵, M. Cordelli³, G. Corradi³, Y. I. Davydov¹, S. Di Falco⁴, E. Diociaiuti³, S. Donati^{4,6}, R.**
9 **Donghia³, B. Echenard², C. Ferrari⁴, A. Gioiosa⁴, S. Giovannella³, V. Giusti⁴, V. Glagolev¹, F.**
10 **Grancagnolo⁷, D. Hampai³, F. Happacher³, D. Hitlin², D. Lin², A. Marini⁴, M. Martini^{3,8}, S.**
11 **Middleton², S. Miscetti³, L. Morescalchi⁴, D. Pasciuto^{4,6,a}, E. Pedreschi⁴, F. Porter², F.**
12 **Raffaelli⁴, A. Saputi³, I. Sarra³, F. Spinella⁴, A. Taffara⁴, G. F. Tassielli⁷, V. Tereshchenko¹, Z.**
13 **Usubov¹, I. I. Vasilyev¹, A. Zanetti⁹, R. Y. Zhu²**

14 ***on behalf of the Mu2e Collaboration***

15 ¹ *Joint Institute for Nuclear Research, Dubna, Russia*

16 ² *California Institute of Technology, Pasadena, California, United States*

17 ³ *Laboratori Nazionali di Frascati dell'INFN, Frascati, Italy*

18 ⁴ *INFN – Sezione di Pisa, Pisa, Italy*

19 ⁵ *ENEA – Frascati, Frascati, Italy*

20 ⁶ *Department of Physics, University of Pisa, Pisa, Italy*

21 ⁷ *INFN – Sezione di Lecce, Lecce, Italy*

22 ⁸ *Department of Engineering Sciences, Guglielmo Marconi University, Rome, Italy*

23 ⁹ *INFN – Sezione di Trieste, Trieste, Italy*

24 *E-mail: daniele.pasciuto@pi.infn.it*

^aCorresponding author.

25 ABSTRACT: The “muon-to-electron conversion” (Mu2e) experiment at Fermilab will search for the
26 Charged Lepton Flavour Violating neutrino-less coherent conversion of a muon into an electron
27 in the field of an aluminum nucleus. The observation of this process would be the unambiguous
28 evidence of the existence of physics beyond the Standard Model. Mu2e detectors comprise a
29 straw-tracker, an electromagnetic calorimeter and an external veto for cosmic rays. In particular,
30 the calorimeter provides excellent electron identification, a fast calorimetric online trigger, and
31 complementary information to aid pattern recognition and track reconstruction. The detector has
32 been designed as a state-of-the-art crystal calorimeter and employs 1348 pure Cesium Iodide (CsI)
33 crystals readout by UV-extended silicon photosensors and fast front-end and digitization electronics.
34 A design consisting of two identical annular matrices (named “disks”) positioned at the relative
35 distance of 70 cm downstream the aluminum target along the muon beamline satisfies the Mu2e
36 physics requirements.

37 The hostile Mu2e operational conditions, in terms of radiation levels (total expected ionizing dose of
38 12 krad and a neutron fluence of 5×10^{10} n/cm² @ 1 MeVeq (Si)/y), magnetic field intensity (1 T) and
39 vacuum level (10^{-4} Torr) have posed tight constraints on scintillating materials, sensors, electronics
40 and on the design of the detector mechanical structures and material choice. The support structure
41 of each 674 crystal matrix is composed of an aluminum hollow ring and parts made of open-cell
42 vacuum-compatible carbon fiber. The photosensors and front-end electronics for the readout of
43 each crystal are inserted in a machined copper holder and make a unique mechanical unit. The
44 resulting 674 mechanical units are supported by a machined plate of vacuum-compatible plastic
45 material. The plate also integrates the cooling system made of a network of copper lines flowing
46 a low temperature radiation-hard fluid and placed in thermal contact with the copper holders to
47 constitute a low resistance thermal bridge. The data acquisition electronics are hosted in aluminum
48 custom crates positioned on the external lateral surface of the disks. The crates also integrate the
49 electronics cooling system as lines running in parallel to the front-end system. In this paper we
50 report on the calorimeter mechanical structure design, the mechanical and thermal simulations that
51 have determined the design technological choices, and the status of component production, quality
52 assurance tests and plans for assembly at Fermilab.

53 **Contents**

54	1 Introduction	1
55	2 The Mu2e Calorimeter	1
56	3 The matrix of CsI Crystals and the Outer Ring	2
57	4 Composite Materials: the Source Plate and the Inner Ring	4
58	5 Plastic Materials: the Back Plate	5
59	6 DAQ Boards and Crates	6
60	7 Plans for Detector Assembly	6
61	8 Conclusions	7

62 **1 Introduction**

63 The Mu2e experiment at Fermilab [1] will search for the Charged Lepton Flavor Violating (CLFV)
64 neutrino-less, coherent conversion of a muon into an electron in the field of an Aluminum nucleus.
65 The experimental signature is a mono-energetic electron with an energy equal to the muon rest mass
66 minus the corrections due to the nuclear recoil and the binding energy. For the Aluminum nucleus,
67 the energy of the mono-energetic electron is approximately 105 MeV. The layout of the Mu2e
68 experiment at Fermilab is thoroughly described in [1]. A system of three superconductive solenoids
69 produces and transports a high intensity pulsed muon beam to the Aluminum target, where muons
70 stop and form muonic atoms. The goal of the Mu2e detectors is detecting the conversion electron
71 from the overwhelming background of particles originated from the standard physics processes
72 which involve the muonic atoms.

73 **2 The Mu2e Calorimeter**

74 The main detectors employed by Mu2e are a straw-tube tracker [2] and an electromagnetic calorime-
75 ter [3] located inside a vessel with a 10^{-4} Torr vacuum level, and surrounded by a large supercon-
76 ducting solenoid which generates an axial magnetic field of 1 T. The main calorimeter function is
77 providing complementary information to the tracker to achieve a powerful μ/e separation which is
78 crucial to extract the conversion electron signal from the expected overwhelming background [4].
79 The calorimeter is also exploited in a calorimeter-seeded track finder algorithm which improves
80 track reconstruction efficiency and makes the algorithm more robust in high detector occupancy
81 conditions. Moreover, the calorimeter is used to implement a fast online standalone trigger indepen-
82 dent from the tracker. These tasks translate into the following requirements for 105 MeV electrons:
83 (a) large geometric acceptance; (b) time resolution better than 500 ps; (c) energy resolution better

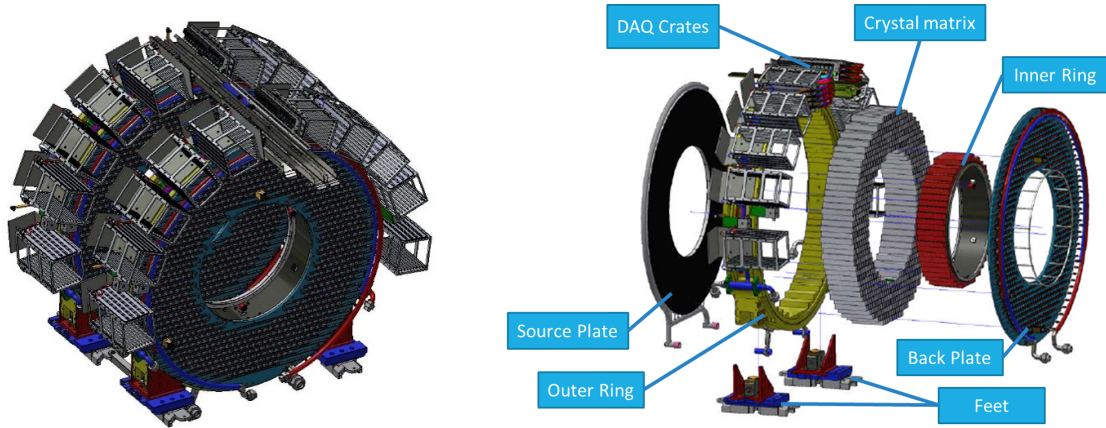


Figure 1. CAD drawings of the Mu2e electromagnetic calorimeter. Global view of the two disks (*left*). Exploded view of one disk: the Outer Ring, the Source Plate, the Crystal Matrix, the DAQ Crates, the Inner Ring, the Back Plate and the Feet are shown (*right*).

84 than 10% and (d) position resolution of the order of 1 cm. The calorimeter has been designed
 85 to maintain a full functionality in the Mu2e very harsh operational conditions: 10^{-4} Torr vacuum
 86 level, 1 T magnetic field, and a very intense particle flux. Depending on the position, a maximum
 87 of Total Ionizing Dose (TID) of the order of 100 krad/year and a neutron fluence of the order of
 88 $10^{12} n_{eq}/cm^2$ are expected over five years of data taking. Since the detectors will be accessible for
 89 maintenance on average only once per year, each calorimeter component is required to be highly
 90 reliable. The presence of the magnetic field requires the use of Silicon PhotoMultipliers (SiPMs)
 91 as photosensors. The required light collection, quantified by Monte Carlo simulation, is at least 20
 92 photo-electrons (p.e.)/MeV. To have a redundant system, each crystal is readout by two photosensors
 93 that collect the light independently. After a long R&D program [5, 6], such requirements pushed
 94 the experiment to adopt a calorimeter made of undoped CsI crystals optically coupled to 14×20
 95 mm^2 large area UV-extended SiPMs. A large SiPM + front-end boards matrix is embedded in the
 96 Back Plate that also integrates a network of cooling lines to control SiPM and front-end electronics
 97 temperature. The DAQ boards are hosted in a battery of 10 crates/disk placed on the disk lateral
 98 surface.

99 The final calorimeter design (Fig. 1) consists of two disks, each containing a matrix of undoped
 100 CsI crystals that are coupled to two SiPMs each. The distance between the two disks is 700 mm
 101 to maximize the acceptance for the 105 MeV signal electrons following a helical trajectory in the
 102 solenoidal magnetic field. A fluorin-rich liquid activated by a neutron generator is fluxed through
 103 a network of pipes housed in the frontal Source Plate to provide the absolute energy scale and the
 104 response equalization among the crystals. A laser system is used to monitor and calibrate SiPM
 105 gains each 1.4 s obtaining an equalization of 0.5%, using fibers enlightening directly each single
 106 crystal/SiPM with the same amount of light.

107 **3 The matrix of CsI Crystals and the Outer Ring**

108 The heart of each of the disks is the ring-shaped matrix of 674 un-doped CsI crystals ($34 \times 34 \times 200$
 109 mm^3) which has an internal/external diameter of 650 mm/1314 mm. Crystals are wrapped in Tyvek
 110 foils (150 μm thick) to improve internal light reflection and separated vertically and horizontally

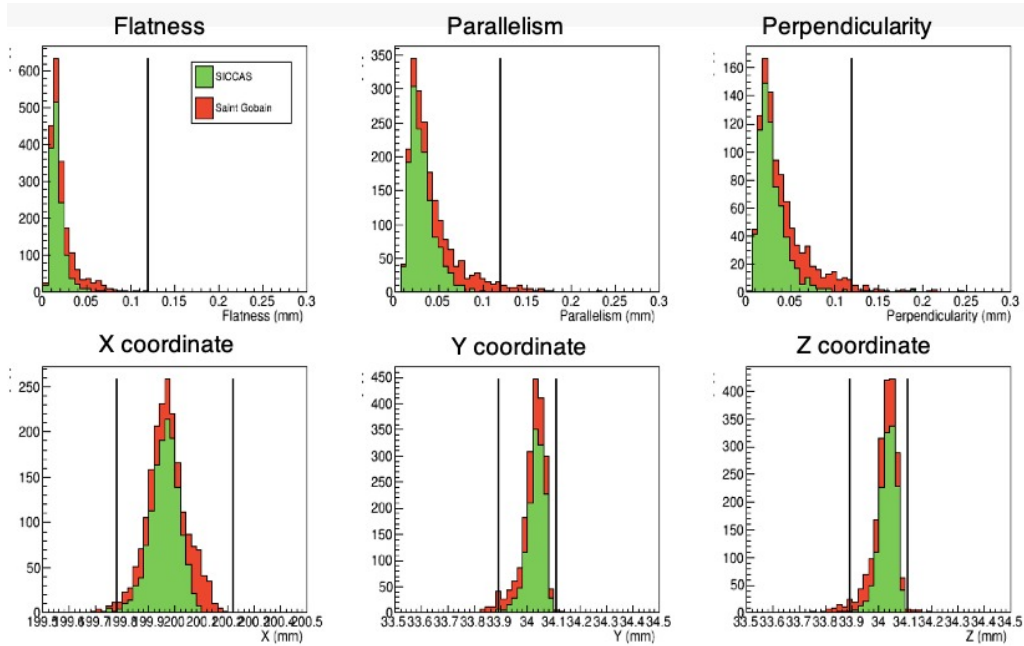


Figure 2. Results of the dimensional quality assurance tests of the production CsI crystals (measurements performed with a CMM at Fermilab). Flatness (*top left*), parallelism (*top center*) and perpendicularity (*top right*) and the X (*bottom left*), Y (*bottom center*) and Z (*bottom right*) dimensions for crystals produced by SICCAS (*green*) and Saint Gobain (*red*). The black vertical lines represent the specification requirements.

111 with black Tedlar foils (50 μm thick) to minimize optical cross-talk.
 112 The crystal quality control procedure was organized as follows: a batch of 60 crystals was shipped
 113 from each producer (Saint-Gobain, France and SICCAS, China) and received at the Fermilab Ship-
 114 ping and Receiving office and then sent to the Mu2e Calorimeter laboratory at SiDet, Lab A [7, 8].
 115 Here, a visual survey excluded the presence of large defects such as large notches, dents, scratches
 116 or bubbles. Then, the mechanical specifications [9] were checked with a Coordinate Measuring
 117 Machine (CMM) model: Brown & Sharpe Global Image 9-15-8. The crystals that did not satisfy the
 118 mechanical requirements were rejected and sent back to the producer. Fig. 2 shows the dimensional
 119 survey results. The accepted crystals were wrapped and the measurements of the optical properties
 120 and Radiation Induced Noise (RIN) were performed [10]. Finally, the crystals were placed in
 121 drawers where N_2 was flown to keep the crystals in a humidity free and controlled environment.
 122 Radiation hardness tests were carried out on a small randomly selected sample in Caltech, Pasadena
 123 (USA) [11, 12].

124
 125 Since crystals are wrapped in Tyvek foils and separated by Tedlar foils, the total envelope of each
 126 crystal is uncertain (tenths of millimeter). We thus performed a series of vertical/horizontal crystals
 127 stacking tests (Fig. 3 left and center). The output was the crystals show an envelope bigger than
 128 the expected because of the multiple material layers used, and a tilting effect which increase with
 129 the height of the stacking column [9]. A model to predict where crystal(i, j) will be located in the
 130 donut-shaped matrix is thus be realized to have a more precise machining of Inner/Outer Ring steps
 131 and SiPM module hollows in the Backplate. For maximum flexibility, the Inner/Outer rings embed
 132 tools for a residual fine-tuning of the crystal positions and alignment with respect to the SiPMs
 133 matrix.

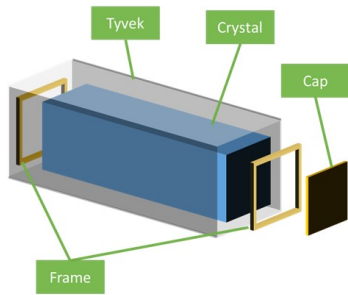


Figure 3. Exploded model of crystal wrapping (*left*). Crystal staggered tower during measurement (*center*). The Outer Ring during the quality assessment at Cerasa Mechanics (Perugia - Italy) (*right*)

134 The crystal matrix is externally supported by the Outer Ring (Fig. 3 right) milled from a bulk block
 135 of Al6082 aluminum to maximize stiffness. The outer diameter and the thickness of the ring are
 136 1460 mm and 146 mm, respectively. The lateral steps are spaced to accommodate and align the
 137 crystals rows. A FEM analysis has been performed considering the weight of the crystal matrix,
 138 pushing the inner surface and of the crates with the digitizing board, pushing the top surface. The
 139 disk leans isostatically on the two feet bulge structures. The maximum ring deformation, i.e. the
 140 vertical ring diameter variation, is of the order of 40 μm , which widely satisfies the calorimeter
 141 dimensional constraints. The Outer Ring also provides all the fastening features for the other
 142 components. It hosts the manifolds for the crate cooling system and supports the DAQ crates on the
 143 lateral surface. The Outer Ring will be inserted in an outer steel frame to transport the calorimeter
 144 from the Sidet laboratory (where the assembly will take place), to the Mu2e experimental site.
 145 The two Outer Rings have been manufactured, and quality controlled. One ring has already been
 146 shipped to Fermilab and is ready for detector assembly while the other one is at INFN National
 147 Laboratory of Frascati to test the assembly procedures.

148 4 Composite Materials: the Source Plate and the Inner Ring

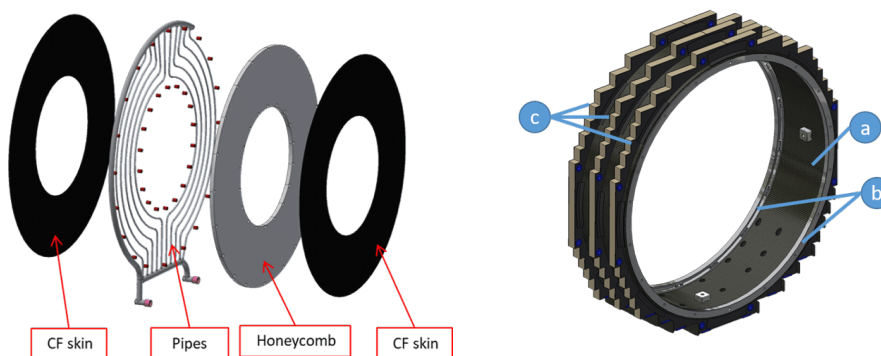


Figure 4. Exploded model of the Source Plate (*left*) and Inner Ring (*right*).

149 The material choice and budget of the mechanical structures that can be traversed by the particles
 150 have been optimized to minimize particle energy losses. The two components placed on the particle

151 trajectories are the Source Panel, which is the frontal cover of the each crystal matrix, and the
152 Inner Ring, which occupies the inner bore surface. They are both made of carbon fiber planes
153 strengthened by light aluminum structures when necessary.

154 The Source Plate (Fig. 4 left) supports 10 thin-wall (0.375" OD x 0.02" thickness) aluminum tubes
155 symmetrically arranged on each disk to flow the calibration source fluid (CF-770). It also provides
156 the frontal enclosure for crystal protection. The Source Plate is made of a sandwich with 1.4 mm
157 carbon fiber skins and a core of aluminum honeycomb (series 3003) 22 mm thick, 3/8" cell size,
158 and 0.003" wall thickness. The expected energy loss is 1.2 MeV for 100 MeV electrons, which is
159 still deemed compatible with Mu2e physics reach [13].

160 The Inner Ring (Fig. 4 right) performs a fundamental function for the support and alignment of the
161 crystal matrix. It is made of:

- 162 • a carbon fiber cylindrical skin with an internal diameter of 712 mm, 4.2 mm thick, an
163 F-.220/193/50 CF fabric (0/90° texture) with cyanate ester resin;
- 164 • two 5083 H111 aluminum alloy reinforcement internal rings with an internal diameter of 672
165 mm, an outer diameter of 712 mm, 13 mm thick to increase its stiffness;
- 166 • three outer step ribs made of a sandwich slab with 1.4 mm carbon fiber skins (same as the
167 cylindrical skin) and a core of aluminum honeycomb (series 3003) 22 mm thick, 3/8" cell
168 size, and 0.003" wall thickness.

169 The Inner Ring is connected and supported by the Back Plate and Source Plate and provides the
170 internal vertical/horizontal reference for the crystal matrix. The Inner Ring also embeds mobile
171 feet which allow to adjust its position and improve the precision of crystal alignment.

172 5 Plastic Materials: the Back Plate

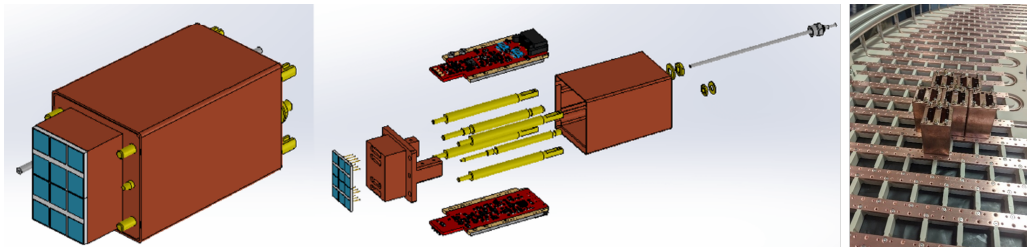


Figure 5. CAD model of a SiPM and Front end electronics holder module (*left and center*). Some prototype modules mounted on the Back Plate (*right*).

173 The Back Plate is the rear mechanical enclosure of the calorimeter. It also supports the 674
174 front-end units which include the SiPMs and front-end electronic boards. The SiPM and front-end
175 electronic modules are composed of 2 SiPMs glued on a copper holder, 2 front-end boards and a
176 copper protective cage (Fig. 5). The modules are fastened directly on the Back Plate Cooling lines
177 to optimize thermal conductivity. The Back Plate is made of a milled PEEK plate (20 mm thick)
178 built by gluing 2 smaller plates with a V-notch joint because of the limited commercial. PEEK was
179 chosen to optimize thermal isolation of the electronics and for its good outgassing characteristics.
180 The Back Plate integrates the cooling system of the front-end units. It embeds a network of vacuum
181 brazed copper lines flowing fluid (3M Novec 649) at -15°C to minimize SiPM dark current and

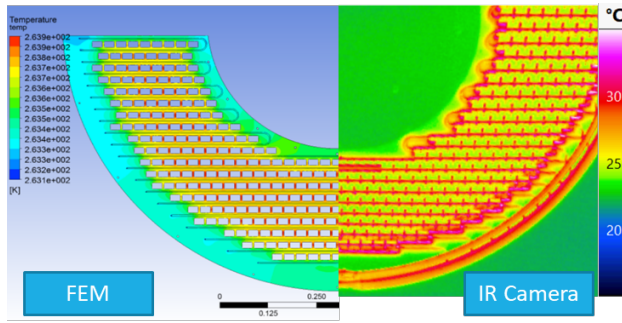


Figure 6. Thermal simulation of the Back Plate and test to check temperature homogeneity (*left*). Back Plate leak tests performed at Cinel (Vigonza - Italy) after manufacturing and assembly (*right*).

182 maintain an acceptable signal/noise ratio over the three years of data taking. Two stainless steel
 183 (AISI 316L) I/O manifolds placed on the external border distribute the cooling fluid among the
 184 network of 38 parallel copper cooling lines embedded in the PEEK to maximize the temperature
 185 uniformity [14]. Tests to verify temperature uniformity have been performed at INFN laboratories
 186 in Pisa by flowing HFE at 50°C (Fig. 6 left). In the same laboratory a geometrical and dimensional
 187 survey has been performed on a gantry shaped Coordinate Measuring Machine (DEA) as part of
 188 the quality control process. Leak tests have been performed at the manufacturer site in Vigonza
 189 (Italy) where a leak rate below $10^{-10} atm cc/s$ has been registered (Fig. 6 right).

190

191 6 DAQ Boards and Crates

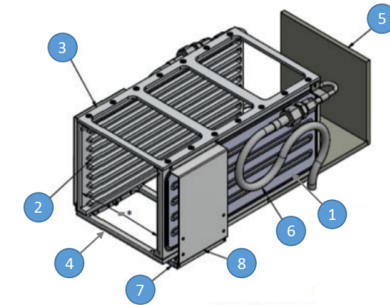


Figure 7. DAQ boards with the copper shield: the Dirac (*green*) and the Mezzanine (*red*) (*left*). CAD Model of the DAQ crate: External side (1), Internal side (2), Top (3), Bottom (4), Tungsten shield(5), Inlet/Outlet pipe (6), Cable holder (7), Cable containment wall (8) (*right*).

192 Each calorimeter disk supports 10 DAQ crates placed on its lateral surface to host 80 DAQ boards
 193 (Digitizer ReAdout Controller (DIRAC) [15] and Mezzanine, Fig. 7 left) which digitize and transmit
 194 the data received from the front-end through optical fibers out of the vessel to the central DAQ
 195 system. Each crate integrates a network of cooling lines to remove the 320 W dissipated by the set
 196 of 8 DAQ boards. To reduce envelopes and optimize the system performance, the cooling lines are
 197 directly carved in the crate sides. Optimal thermal contact between the electronic components and
 198 the heat sink is achieved through a machined copper plate positioned on top of the DAQ boards
 199 and placed in thermal contact with the components with vacuum proof thermal grease (Apiezon).

200 The DAQ crate structure (Fig. 7 right) is completed by a set of tungsten plates which protect the
201 electronic components from the high level of radiation present in experimental area at run time.
202 Thermal simulations and experimental tests have been performed in air as well as in vacuum to
203 crosscheck the cooling system performance [16]. The DAQ crates production is now progressing.

204 7 Plans for Detector Assembly



Figure 8. Photograph of the cleanroom for detector assembly at SiDet Laboratory - Fermilab (*left*). Photograph of the Outer Ring and Back Plate assembled at INFN National Laboratory of Frascati (*right*).

205 The calorimeter will be assembled in a 10000-class cleanroom built in the SiDet Laboratory at
206 Fermilab (Fig. 8 left). Two assembly stations will be available to test the first assembled disk
207 while building the second one. An assembly station has been realized also at the INFN National
208 Laboratory of Frascati to test the components received from the vendors before shipment to Fermilab
209 (Fig. 8 right). Outgassing tests of the components will be performed before assembly in dedicated
210 vessels (the most critical components are crystals and cables) and the alignment of the crystal matrix
211 will be continuously monitored during detector assembly. Tests of the cooling system and electronic
212 components will be continuously performed during and after detector assembly.

213 8 Conclusions

214 The design of the Mu2e electromagnetic calorimeter mechanical structures has been finalized after
215 many years of research and development. At the time of writing this paper, most components have
216 been built and are now being tested for quality assurance. The production and quality assurance
217 of the Cesium Iodide crystals and silicon photomultipliers have been completed. The production
218 of the front-end electronics has been completed, whereas data acquisition electronics is currently
219 progressing. The detector assembly is expected to be completed in 2022.

220 Acknowledgments

221 We are grateful for the vital contributions of the Fermilab staff and the technical staff of the
222 participating institutions. This work was supported by the US Department of Energy; the Istituto
223 Nazionale di Fisica Nucleare, Italy; the Science and Technology Facilities Council, UK; the Ministry
224 of Education and Science, Russian Federation; the National Science Foundation, USA; the Thousand
225 Talents Plan, China; the Helmholtz Association, Germany; and the EU Horizon 2020 Research and

226 Innovation Program under the Marie Skłodowska-Curie Grant Agreement No. 690385 ,734303,
227 822185, 858199, 101003460. This document was prepared by members of the Mu2e Collaboration
228 using the resources of the Fermi National Accelerator Laboratory (Fermilab), a U.S. Department
229 of Energy, Office of Science, HEP User Facility. Fermilab is managed by Fermi Research Alliance,
230 LLC (FRA), acting under Contract No. DE-AC02-07CH11359.

231 References

- 232 [1] L. Bartoszek et al., *Mu2e Technical Design Report*, (2014) arXiv:1501.05241
- 233 [2] M.Lee and the Mu2e collaboration, *The Straw Tube tracker for the Mu2e experiment*, Nuclear and
234 Particle Physics proceedings 273-275 (2016)
- 235 [3] N. Atanov et al., *The calorimeter of the Mu2e experiment at Fermilab*, JINST 12 (01) (2017), C01061.
- 236 [4] N. Atanov et al., *Design and Status of the Mu2e Crystal Calorimeter*, IEEE TRANSACTIONS ON
237 NUCLEAR SCIENCE, VOL. 65, NO. 8, p.2073-2080, AUGUST 2018
- 238 [5] N. Atanov et al., *Measurement of time resolution of the Mu2e LYSO calorimeter prototype*,
239 Nucl.Instrum.Meth. A812 (2016), 104-111.
- 240 [6] O. Atanova et al., *Measurement of the energy and time resolution of a undoped CsI + MPPC array for*
241 *the Mu2e experiment*, JINST 12 (2017) no.05, P05007.
- 242 [7] D. Pasciuto on behalf of the Mu2e calorimeter group, *Calo QA Lab at SiDet, Info and documents*,
243 Internal report: Mu2eDoc16988
- 244 [8] N. Atanov et al., *The Mu2e e.m. Calorimeter: Crystals and SiPMs Production Status*, IEEE
245 TRANSACTIONS ON NUCLEAR SCIENCE, VOL. 67, NO. 6, p.978-982, JUNE 2020
- 246 [9] D. Pasciuto, *Physical and mechanical properties study of CsI scintillation crystals and design of the*
247 *mechanical structure for the Mu2e Electromagnetic Calorimeter at Fermilab*, PhD Thesis, Università
248 degli studi Guglielmo Marconi (2020-2021)
- 249 [10] N. Atanov et al., *Quality assurance on undoped CsI crystals for the Mu2e experiment*, IEEE
250 Transactions on Nuclear Science 65.2 (2017): 752-757
- 251 [11] E. Diociaiuti, *Study of the Mu2e sensitivity to the $\mu^- \rightarrow e^+$ conversion process*, PhD Thesis, Università
252 degli studi Tor Vergata (2019-2020).
- 253 [12] M. Cordelli et al., *Summary of CsI crystals production and related QA tests*, Internal presentation:
254 Mu2eDoc35564
- 255 [13] N. Atanov et al., *The Mu2e Calorimeter Final Technical Design Report*, TDR (2018)
256 arXiv:1802.06341
- 257 [14] L. Morescalchi et al., *Automated Test Station for the Characterization of Custom Silicon*
258 *PhotoMultipliers for the Mu2e Calorimeter*, PoS TWEPP2018 (2019) 017 10.22323/1.343.0017
- 259 [15] E. Pedreschi et al., *The Digitizer ReAdout Controller (DIRAC) of the Mu2e electromagnetic*
260 *calorimeter at Fermilab*, PoS TWEPP2019 (2020) 119, 10.22323/1.370.0119
- 261 [16] E. Benedetti, *Design and thermal analysis of the Mu2e experiment calorimeter*, Master Thesis,
262 Università di Pisa (2017-2018).